

Attribution-NonCommercial-NoDerivatives 4.0 International (CC BY-NC-ND 4.0)
<https://creativecommons.org/licenses/by-nc-nd/4.0/>

Access to this work was provided by the University of Maryland, Baltimore County (UMBC) ScholarWorks@UMBC digital repository on the Maryland Shared Open Access (MD-SOAR) platform.

Please provide feedback

Please support the ScholarWorks@UMBC repository by emailing scholarworks-group@umbc.edu and telling us what having access to this work means to you and why it's important to you. Thank you.

Deep PIM kinase substrate profiling reveals new rational co-therapeutic strategies for acute myeloid leukemia

Tracking no: ADV-2022-008144R1

Tejashree Joglekar (University of Maryland, Baltimore County, United States) Alexander Chin (University of Maryland, Baltimore County, United States) Alin Voskian-Kordi (University of Maryland, Baltimore County, United States) Baek Seungchul (University of Maryland, Baltimore County, United States) Azim Raja (University of Maryland, Baltimore County, United States) Apurv Rege (University of Maryland, Baltimore County, United States) Weiliang Huang (University of Maryland, Baltimore, United States) Maureen Kane (University of Maryland,) Marikki Laiho (Johns Hopkins University School of Medicine, United States) Thomas Webb (Wildflower Biopharma, Inc., United States) Xiaoxuan Fan (University of Maryland Greenebaum Comprehensive Cancer Center, United States) Michael Rubenstein (University of Maryland, Baltimore County, United States) Charles Bieberich (University of Maryland, Baltimore County, United States) Xiang Li (University of Maryland, Baltimore County, United States)

Abstract:

Provirus integration site for Moloney murine leukemia virus (PIM) family serine/threonine kinases perform pro-tumorigenic functions in hematologic malignancies and solid tumors by phosphorylating substrates involved in tumor metabolism, cell survival, metastasis, inflammation, and immune cell invasion. However, a comprehensive understanding of PIM kinase functions is currently lacking. Multiple small molecule PIM kinase inhibitors are currently being evaluated as co-therapeutics in cancer patients. To further illuminate PIM kinase functions in cancer, we deeply profiled PIM1 substrates using the reverse in-gel kinase assay to identify downstream cellular processes targetable with small molecules. Pathway analyses of putative PIM substrates nominated RNA splicing and rRNA processing as PIM-regulated cellular processes. PIM inhibition elicited reproducible splicing changes in PIM-inhibitor-responsive acute myeloid leukemia (AML) cell lines. PIM inhibitors synergized with splicing modulators targeting splicing factor 3b subunit 1 (SF3B1) and serine-arginine protein kinase 1 (SRPK1) to kill AML cells. PIM inhibition also altered rRNA processing, and PIM inhibitors synergized with an RNA polymerase I inhibitor to kill AML cells and block AML tumor growth. These data demonstrate that deep kinase substrate knowledge can illuminate unappreciated kinase functions, nominating synergistic co-therapeutic strategies. This approach may expand the co-therapeutic armamentarium to overcome kinase-inhibitor resistant disease that limits durable responses in malignant disease.

Conflict of interest: No COI declared

COI notes:

Preprint server: No;

Author contributions and disclosures: Conceptualization, T.J., A.C., X.L., and C.J. B.; investigation, T.J., A.C., X.L., A.R., W.H. and A.R.; formal analysis, T. J., A.C., W.H., X.L., A. V-K., M.R., B.S., X.F. and C.J.B.; resources, T.W. M.L., and M.K.; writing - original draft, T.J., X.L., and C.J. B.; writing - review & editing, all authors; funding acquisition, X.L. and C.J.B.

Non-author contributions and disclosures: No;

Agreement to Share Publication-Related Data and Data Sharing Statement: Microarray data is available here: <https://umbc.box.com/s/8lrvo3mlj0qy9fik2n7xvkd7lx0e4yhx>. All other data and reagents are available from the corresponding author upon request.

Clinical trial registration information (if any):

Deep PIM kinase substrate profiling reveals new rational co-therapeutic strategies for acute myeloid leukemia

Tejashree Joglekar¹, Alexander Chin¹, Alin Voskanian-Kordi¹, Baek Seungchul², Azim Raja¹, Apurv Rege¹, Weiliang Huang³, Maureen Kane³, Marikki Laiho⁴, Thomas R. Webb⁵, Xiaoxuan Fan^{6,7}, Michael Rubenstein¹, Charles J. Bieberich^{1,6,*} and Xiang Li^{1*}

¹Department of Biological Sciences, University of Maryland, Baltimore County, Baltimore, MD 21250

²Department of Mathematics and Statistics, University of Maryland, Baltimore County, Baltimore, MD 21250

³Department of Pharmaceutical Sciences, University of Maryland, Baltimore, Baltimore MD 21201

⁴Department of Radiation Oncology and Molecular Radiation Sciences, Johns Hopkins University School of Medicine, Baltimore, Maryland 21287

⁵Wildflower Biopharma, Inc., www.wildflowerbiopharma.com

⁶Department of Microbiology and Immunology, University of Maryland Baltimore School of Medicine, Baltimore, MD 21201

⁷University of Maryland Marlene and Stewart Greenebaum Comprehensive Cancer Center, Baltimore, MD 21201

*Correspondence bieberic@umbc.edu; lixiang@umbc.edu

Data sharing statement

Microarray data is available here:

<https://umbc.box.com/s/8lrvo3m1j0qy9fik2n7xvgd7lx0e4yhx>. All other data and reagents are available from the corresponding author upon request.

Running title: PIM kinases control splicing and ribosome biogenesis

Word count: 3998

Number of figures/tables: 5 main; 6 supplemental

Number of references: 65

Key Points

1. Proteomic profiling of PIM kinase substrates identifies RNA splicing and ribosome biogenesis as PIM-controlled cellular processes.
2. PIM inhibitors alter RNA splicing and rRNA processing and synergize with splicing modulators and an RNA polymerase I inhibitor to kill AML cells.

Abstract

Provirus integration site for Moloney murine leukemia virus (PIM) family serine/threonine kinases perform pro-tumorigenic functions in hematologic malignancies and solid tumors by phosphorylating substrates involved in tumor metabolism, cell survival, metastasis, inflammation, and immune cell invasion. However, a comprehensive understanding of PIM kinase functions is currently lacking. Multiple

small molecule PIM kinase inhibitors are currently being evaluated as co-therapeutics in cancer patients. To further illuminate PIM kinase functions in cancer, we deeply profiled PIM1 substrates using the reverse in-gel kinase assay to identify downstream cellular processes targetable with small molecules. Pathway analyses of putative PIM substrates nominated RNA splicing and rRNA processing as PIM-regulated cellular processes. PIM inhibition elicited reproducible splicing changes in PIM-inhibitor-responsive acute myeloid leukemia (AML) cell lines. PIM inhibitors synergized with splicing modulators targeting splicing factor 3b subunit 1 (SF3B1) and serine-arginine protein kinase 1 (SRPK1) to kill AML cells. PIM inhibition also altered rRNA processing, and PIM inhibitors synergized with an RNA polymerase I inhibitor to kill AML cells and block AML tumor growth. These data demonstrate that deep kinase substrate knowledge can illuminate unappreciated kinase functions, nominating synergistic co-therapeutic strategies. This approach may expand the co-therapeutic armamentarium to overcome kinase-inhibitor resistant disease that limits durable responses in malignant disease.

Introduction

Deregulation of kinase signaling networks is a common feature of nearly all malignancies [1]. Targeting these networks using small molecule drugs, principally kinase inhibitors (KIs), is revolutionizing cancer therapy [2]. However, the promise of this therapeutic approach is tempered by the reality that durable responses are limited in most patients by the emergence of drug-resistant disease[3]. KI resistance develops through multiple molecular mechanisms that re-activate the targeted signaling pathway

including kinase mutations that preclude drug binding, activation of downstream signaling, and upregulation of compensatory signaling pathways [4]. These changes can emerge through *de novo* alterations in the bulk tumor cell population induced by therapeutic pressure or through selection of pre-existing subclones owing to cancer cell heterogeneity. Kinase inhibitor polypharmacology approaches, wherein multiple signaling pathways are simultaneously inhibited, are widely anticipated to extend time to relapse by increasing the roadblocks that must be circumvented to permit cancer cell survival. However, choosing efficacious drug combinations remains a critical challenge [4]. For well-characterized pathways, it may be feasible to target multiple components of a single pathway to prevent downstream signaling re-activation. A prominent exemplar of this strategy is the combination of B-raf inhibitors and mitogen-activated protein kinase (MEK) inhibitors in B-raf V600E-mutant melanomas [5]. In cases where compensatory signaling that fuels resistance has been defined, increased therapeutic efficacy can also be achieved by simultaneously targeting the driver and compensating pathways. For example, in triple negative breast cancer, MEK inhibition leads to upregulation of several receptor tyrosine kinases (RTKs) that activate extracellular signal-regulated protein kinase (ERK). Combining MEK inhibitors with sorafenib, which targets multiple RTKs, led to increased tumor growth inhibition [6].

Where such rational choices are less obvious, high throughput combinatorial drug screens and genetic approaches that illuminate drug-phenotype relationships may be informative [7,8]. Recently, patient-individualized systems approaches that combine *in silico* prediction and *ex vivo* analyses of patient samples have identified synergistic combinations among 218 compounds including kinase inhibitors [9].

From the examples cited above, it is axiomatic that knowledge of kinase signaling input and output is central to rationalizing potential drug combinations to inform multi-hit strategies on a single pathway, to combat compensatory signaling and to train systems-level algorithms. In terms of output, knowledge of direct physiological kinase substrates provides a clear route to elucidating signaling outcomes and rationalizing drug combinations, as in the case of B-raf and MEK inhibitors. Multiple biochemical and genetic approaches have been developed to profile protein kinase substrates [10]. Despite substantial progress in our understanding of kinase-substrate interactions, comprehensive substrate repertoires are lacking even for the most well-studied kinases [11]. This partial knowledge of a key dimension of kinase biology [12] restricts our ability to rationalize co-therapeutics for many kinase inhibitors.

Reasoning that deepened knowledge of direct kinase-substrate interactions would nominate new rational KI co-therapeutic strategies, we sought to comprehensively profile substrates of a well-studied oncogenic kinase family in a leukemia cell line. PIM kinases have long been known to be drivers of oncogenesis in AML and to augment oncogenic processes in other malignancies [13,14]. PIM1, 2, and 3 are constitutively active serine threonine kinases and triple loss-of-function affects growth but not viability or fertility in mice [15]. This dispensability positions them as attractive therapeutic targets, and multiple small molecule PIM kinase inhibitors have been tested or are currently under evaluation in clinical trials for cancer treatment [16]. PIM kinases are known to directly phosphorylate substrates involved in cell cycle progression, survival, translation, transcription, and drug resistance, and this knowledge has been leveraged to suggest rational, mechanism-based drug combinations that have

shown considerable preclinical promise against multiple forms of cancer [17]. PIM kinases have also been strongly implicated in the emergence of therapeutic resistance in cancer through multiple mechanisms including direct phosphorylation of drug transporters [18–21].

Here, we describe a high-throughput iteration of the reverse in-gel kinase assay, and demonstrate, using PIM1 as a paradigm, that broadening understanding of kinase-substrate interactions identifies previously underappreciated cellular processes under kinase control, and efficiently nominates rational drug combinations that synergize to block AML cell growth. Extending this approach to other oncogenic driver and supportive kinases has the potential to considerably expand therapeutic options to delay time to relapse and extend overall survival in AML and other cancers treated with KIs.

Methods

Cell culture

All cell lines were maintained at 5% CO₂ and 37°C. Culture media was supplemented with antibiotics, antimycotics and anti-mycoplasma agents.

Recombinant Proteins

PIM1 and PIM2 genes (Open Biosystems) were cloned into pQE-80L and expressed in *E. coli* BL21. Recombinant PIM kinases were purified using nickel resin. Recombinant PIM substrates were generated by cloning cDNAs from HeLa RNA into pQE-80L and purified as described above for PIM kinases.

Reverse In-gel kinase assays (RIKA)

RIKAs were performed essentially as described [22]. For shotgun RIKAs, ~1 mg HF-treated K562 protein extract was analyzed in each of four 5 ml RIKA gels containing PIM1 (50 ug/ml). Hydrogen fluoride (HF) treatment was used to dephosphorylate and deglycosylate proteins as described [23]. RIKA gels were cut into 8 sections, and sections of the same molecular weight from all four gels were combined and homogenized in 50 mM NaHCO₃. Phosphopeptides were enriched using a titanium dioxide resin kit (Pierce).

nanoUPLC-tandem mass spectrometry analysis of phosphopeptidome

Titanium dioxide-enriched tryptic phosphopeptides were separated on a nanoACQUITY UPLC analytical column (BEH130 C18, 1.7 µm, 75 µm x 150 mm, Waters) over a 95-minute linear acetonitrile gradient (3 – 35%) with 0.1 % formic acid on a Waters nano-ACQUITY UPLC system and analyzed on a coupled Thermo Scientific Orbitrap Fusion Tribrid mass spectrometer. Full scans were acquired at a resolution of 120,000, and precursors were selected for fragmentation by a real-time data-dependent decision tree (DDDT) logic based on the precursor charge state and m/z using higher-energy collisional dissociation (HCD, normalized collision energy at 30%) or electron-transfer dissociation (ETD) for a maximum 3-second cycle as described by Swaney *et al.* [24]. Tandem mass spectra were searched against UniProt Homo sapiens reference proteome using Sequest HT algorithm described by Eng *et al.* [25] and MS Amanda algorithm developed by Dorfer *et al.* [26] with a maximum precursor mass error tolerance of 10 ppm. Phosphorylations of serine and threonine (monoisotopic mass change

+79.9663 Da) were treated as dynamic modifications. Resulting hits were validated at a maximum false discovery rate of 0.01 using a semi-supervised machine learning algorithm Percolator developed by Käll *et al.* [27]. The probabilities of phosphorylation sites were calculated by using phosphoRS algorithm developed by Taus *et al.* [28] .

Inhibitor treatment

AZD1208 (pan-PIM inhibitor) (MedKoo Biosciences, #205763), PIM447 (pan-PIM inhibitor) (MedChemExpress #HY-19322B), LY2584702 (p70S6 kinase Inhibitor) (Selleck chemicals, #S7704), Pladienolide B (SF3B complex inhibitor) (Santacruz Biotechnology, #445493-23-2) SPHINX31 (SRPK1 inhibitor) (MedChemExpress, #HY-117661) and Sudemycin D6 (SD6) were solubilized in DMSO. BMH-21 was provided as pre-solubilized in citrate buffer (pH 6). For vehicle treatment, a solvent volume equal to the volume of inhibitor stock solution was used.

MTT assays

Metabolic activity was quantified using MTT (GoldBio, #T-030) by measuring OD at 570 nm on a Biotek Synergy 2 plate reader. FA values were determined using CompuSyn (<http://www.combosyn.com>) to calculate the combination indices (CI values) at ED50, ED75, ED90 and ED95 (ED- Effective dose of combination).

Flow cytometry

EOL-1 cells were treated with DMSO, PIM inhibitor, SRPK1 inhibitor, or combination of PIM and SRPK1 inhibitors for 48 hours. Cells were seeded 24 hours prior to treatment.

Cells were harvested and resuspended in cold Annexin-binding buffer (Thermofisher, #V13241) to a cell density of $\sim 2 \times 10^6$ cells/mL. Cells were stained with Annexin V-Alexa Fluor 647 (Thermofisher, #A23204) and Propidium Iodide (PI) on ice for 10 minutes. Flow cytometry was performed on BD FACSCanto II cytometer equipped with 488 nm and 633 nm lasers. 50,000 singlet events from two biological replicates of each treatment condition were recorded in duplicate. Compensation was performed based on single color control cells stained with Annexin V or PI alone. Data analysis was performed using FCSEXPRESS 7 (version 7.16, De Novo Software). Statistical analysis was performed using one-way ANOVA followed by multiple comparisons test with Tukey's correction on GraphPad Prism (version 10.1.1).

Microarray analysis of RNA splicing

RNA samples extracted from AML cell lines with, and without, AZD1208 treatment were analyzed on Affymetrix GeneChipTM Human Transcriptome Analysis 2.0 (HTA 2.0) microarrays. Data was analyzed using Transcriptome Analysis Console (TAC) software using CHP files from three biological replicates.

RT-PCR analysis

cDNA from DMSO control-treated and inhibitor-treated AML cell lines was analyzed by RT-PCR to interrogate changes in CHAC1 splicing. Primers were designed by querying mRNA sequences using the NCBI nucleotide reference sequence database (RefSeq). NCBI/Primer-BLAST was used to identify primers that recognized sequences flanking alternatively spliced exons. MCL1 transcripts MCL-1L (assay name: Hs00172036_m1)

and MCL-1S (assay name: Hs00766187_m1) were quantified using TaqMan™ assays (ThermoFisher Scientific). 30 ng of total cDNA was used for each reaction. GAPDH (assay name: Hs99999905_m1) was used as a loading control. A CFX96 Touch™ real-time PCR detection system was used for the reaction. Each sample was tested in triplicates, No-RT controls were also tested in triplicate for each RNA sample with each probe reaction. Data analysis was performed using the BioRad CFX Manager™ and CFX Maestro software. Ratios of MCL-1S to MCL-1L were quantified, and statistical analysis was performed using one-way ANOVA, with corrected standard deviations, followed by multiple comparisons test with Tukey's correction on GraphPad Prism (version 10.1.1).

Analysis of rRNA precursors

MOLM-16, EOL-1 and OCI-M1 cells were treated with PIM inhibitor (AZD1208 or PIM447) or S6 Kinase inhibitor (LY2584702). RNA (5 µg) was resolved on 0.9% Agarose gels in 1X NorthernMax® Gly gel prep/running buffer (Ambion), transferred to Nytran™ membranes (GE Whatman™ 10416096) and crosslinked UV irradiation. Northern blot analysis for rRNA precursors was performed essentially as described (Tafforeau et al., 2013).

Western blotting

Cells were lysed in denaturing buffer containing urea (7M Urea, 2M thiourea, 20mM DTT, 1%C7BZ0, 20mM Tris pH 7.5) and resolved proteins were transferred to PVDF membranes. Phospho-rpS^{235/236} antibody (Cell signaling technology, #4858) was used.

***In vivo* analysis of drug efficacy**

5 X 10⁶ EOL-1 cells in PBS were injected subcutaneously in the flank of 8-12 week-old NOD.Cg-*Prkdc*^{scid} *Il2rg*^{tm1Wjl}/SzJ (NSG) male and female mice (Jackson Lab strain 005557). Tumor volume was measured every other day until tumor volume reached 1500 mm³ (IACUC-mandated endpoint for euthanasia).

The animal studies were performed under a protocol approved by the Institutional Animal Care and Use Committee of the University of Maryland, Baltimore County.

Results

Shotgun RIKA identifies >450 new potential PIM kinase substrates

Protein kinase substrates can be identified and phosphorylation stoichiometry can also be accurately quantified using the reverse in-gel kinase assay (RIKA), however assay throughput is low [22,29]. To accelerate kinase substrate discovery, we developed a “shotgun” RIKA (Figure 1A). K562 CML whole cell protein extracts were first quantitatively dephosphorylated and deglycosylated using hydrogen fluoride (HF) [23] and resolved on a denaturing sodium dodecyl sulfate polyacrylamide gel with recombinant 33 kDa PIM1S (hereafter, PIM1) polymerized within, and a parallel control gel without PIM1. After in-gel protein refolding, in-gel kinase assays were performed. Both gels were then divided into eight regions based on apparent molecular weight, tryptic peptides were extracted, and phosphopeptides were enriched by TiO₂ chromatography. Eluted phosphopeptides were fractionated by reverse-phase LC and

analyzed using high resolution MS/MS. 1035 phosphopeptides present exclusively in the PIM1-containing gel were mapped to 778 putative PIM1 substrate proteins using Proteome Discoverer [30] to query the Uniprot database (FDR <0.05, Table S1). Of these, 461 were not previously reported as PIM substrates [31,32]. DAVID pathway analysis [33] demonstrated a strong link between PIM kinase substrates and RNA biology (Figure 1B). Ribosome, spliceosome, RNA transport, ribosome biogenesis, mRNA surveillance and RNA degradation were among the top 13 DAVID hits (Figure 1B). To confirm specific RNA-linked and other pathway (*i.e.* cell cycle control and DNA repair) components as PIM kinase substrates, full-length recombinant proteins produced in *E. coli* were analyzed in standard ^{32}P -ATP RIKAs [22]. 19 of 20 were phosphorylated with high catalytic efficiency. 6 are shown in Fig. 1C and the remainder in Fig S1. ~~(Figs. 1C & S1).~~ These data demonstrate that this high throughput workflow accurately identifies, in the vast majority of cases, proteins that are robust *in vitro* PIM substrates.

PIM kinase inhibition profoundly and reproducibly alters RNA splicing

Among the 461 novel PIM substrates, three core mRNA splicing components (BUD13, SF3A1, U2AF1) and seven auxiliary splicing factors (SRSF1, SRSF2, SRSF5, SRSF6, SRSF7, SRSF9, and SRSF10) were observed, suggesting that PIM kinases may control mRNA splicing. To determine if modulating PIM activity alters mRNA splicing patterns, PIM inhibitor-responsive MOLM-16 and EOL-1 acute myeloid leukemia cell lines were treated with the pan-PIM inhibitor (R,Z)-5-((2-(3-aminopiperidin-1-yl)-[1,1'-biphenyl]-3-yl)methylene)thiazolidine-2,4-dione (AZD1208) for six hours and microarray

analyses (HTA 2.0, Affymetrix) were performed. 2,427 quantitative changes in alternative splicing events mapping to 1093 genes were observed in both cell lines (Table S2). Importantly, the direction of change in these splicing events was concordant in the vast majority of cases, as indicated by quadrant plotting (Figure 2A). Among alternative splicing events, exon skipping/inclusion predominated, followed by alternative 5' donor and 3' acceptor usage (Figure 2B). Intron retention was the least frequently observed event (Figure 2B). To validate the PIM inhibitor-inducibility of specific splicing events predicted by the microarray data, RT-PCR analyses were performed. TaqMan qRT-PCR analyses to quantify the long and short myeloid cell leukemia-1 (MCL-1) mRNA isoforms demonstrated a significant increase in the MCL-1L:MCL-1S ratio as observed in the microarray analysis in MOLM-16 cells (Figure 2C). Likewise, semi-quantitative RT-PCR analysis of glutathione-specific gamma-glutamylcyclotransferase 1 (CHAC1) mRNA isoforms concordant with the microarray data were also observed (Figure 2D). To demonstrate that AZD1208-induced changes in MCL-1 and CHAC1 splicing are not due to off-target effects of AZD1208, AML cells were treated with N-[4-[(1R,3S,5S)-3-amino-5-methylcyclohexyl]pyridin-3-yl]-6-(2,6-difluorophenyl)-5-fluoropyridine-2-carboxamide (PIM447). Essentially identical changes in MCL-1 and CHAC1 mRNA splicing in MOLM-16 were observed by RT-PCR (Figure 2C,D). Similar changes in MCL-1 and CHAC1 splicing were also observed by RT-PCR in AZD1208- and PIM447-treated EOL1 cells (Figure 2C,D), despite not being detected as significant in the microarray analysis. These data demonstrate that PIM kinase blockade, using two chemically distinct small molecule inhibitors, results in extensive alterations in specific mRNA isoform abundance in PIM inhibitor-sensitive AML cells. In

contrast, no consistent changes in MCL1 splicing were observed in drug-treated AZD1208-resistant OCI-M1 cells[34] (Figure S3A,B).

PIM kinase inhibition synergizes with splicing disruptors to kill AML cells

Alternative splicing has recently been identified as a therapeutic vulnerability in AML and other cancers. Recurrent hotspot mutations have been identified in three spliceosome components (SF3B1, SRSF2, U2AF1) in multiple hematologic malignancies including AML [35]. These mutations lead to altered splice site recognition. Interestingly, in AML, spliceosome mutations are almost always heterozygous and mutually exclusive. This suggests that while some degree of spliceosome component perturbation may be pro-oncogenic, further alteration may be incompatible with viability [36]. We therefore reasoned that PIM inhibition might induce chemical synthetic lethality in SF3B1 wild-type cells by providing a first 'hit' to alternative splicing, rendering them more susceptible to SF3B1-targeting agents. To test this hypothesis, we determined, using 3-(4,5-dimethylthiazol-2-yl)-2,5-diphenyltetrazolium bromide (MTT) assays, the effects of combining PIM inhibition with the SF3B1 inhibitors pladienolide B [37] or Sudemycin D6 [38]. Combination indices (CI values) were determined using the Chao-Talalay median-effect equation [39] for combinations of AZD1208 plus the SF3B1 inhibitors pladienolide B [37] or Sudemycin D6 [38]. Synergy in the AZD1208 plus pladienolide B and the AZD1208 plus Sudemycin D6 combinations was observed in both MOLM-16 and EOL-1 cell lines (Figure 3A).

In addition to SF3B1-targeting agents, inhibitors of splicing kinases are also being developed as splicing-targeting therapeutics. Serine arginine protein kinases

1-3 (SRPK1-3) phosphorylate serine-arginine rich (SR) proteins in the cytoplasm to facilitate transport to the nucleus where they regulate splice site selection [40]. SRPK1 also facilitates SR protein release from CDC2-like kinase 1-SR protein complexes in the nucleus [41]. Genetic and pharmacologic SRPK1 inhibition has been shown to alter splicing and block growth in MLL-rearranged acute myeloid leukemias (AML) [42,43]. To determine if PIM kinase inhibition would synergize with the SRPK1 inhibitor SPHINX31, MLL-rearranged AML EOL-1 and MV4-11 cells and MLL-WT MOLM-16 cells were treated with the combination [43]. Very strong synergy in cell killing was observed in EOL-1 and MV4-11 (Figure 3B). To further explore the cellular basis of the observed synergy, flow cytometry and Trypan Blue exclusion analyses were performed in EOL1 cells (Figure. S2). As expected, PIM kinase and SRPK1 inhibition alone increased the population of apoptotic and dead cells. The combination significantly increased that population (Figure S2).

PIM kinase inhibition alters rRNA processing and synergizes with ribosome biogenesis disruptors to kill AML cells

In addition to mRNA splicing, pathway analysis also nominated ribosome biology as a major PIM target of PIM activity (Figure 1B). PIM inhibition is known to alter protein translation but has not been reported to affect ribosome biogenesis [44]. Systematic comparison of the RIKK-generated PIM substrate profile to a database of 286 validated rRNA processing factors (exclusive of ribosomal proteins) revealed 50 PIM substrates known to be validated rRNA processing factors [45]. To determine whether PIM inhibition alters rRNA processing in AML, pre-rRNA abundance was quantified by

Northern blot analyses of rRNA from AZD1208-treated MOLM-16 and EOL-1 cells. rRNA processing was reproducibly perturbed at multiple steps, resulting in accumulation of 30S pre-rRNA, reduction of 26S, 21S and 18S-E pre-rRNAs and appearance of an aberrant rRNA intermediate larger than the 18S-E pre-rRNA (Figure 4). In contrast, PIM inhibition in AZD1208-resistant OCI-M1 cells failed to induce detectable rRNA processing changes (Figure S3C). To demonstrate that AZD1208-induced changes in rRNA processing are not due to off-target effects of AZD1208, MOLM-16 cells were treated with PIM447, and identical changes in pre-rRNA processing were observed (Figure S4A). These data demonstrate that PIM inhibition alters specific steps in rRNA processing. In contrast, inhibition of S6 kinase, a well-known regulator of ribosome biogenesis, with LY2584702 in MOLM-16 cells did not induce rRNA processing changes, despite a clear decrease in pRPS6-S²³⁵⁻²³⁶ upon LY2584702 treatment (Figure S4B,C). These data demonstrate that PIM inhibition profoundly and specifically alters rRNA processing at multiple steps, strongly suggesting that PIM kinases regulate a key step in ribosome biogenesis.

The identification of ribosome biogenesis as a PIM-inhibitor responsive pathway suggested that combining PIM inhibition with disruptors of this pathway could potentially synergize. To test this hypothesis, we determined the effects of co-targeting PIM kinases and RNA Polymerase I (Pol I) or S6 Kinase. Combination indices (CI values) determined using the Chao-Talalay median-effect equation for combinations of PIM inhibitors plus the RNA pol I inhibitor BMH-21 [46], or the S6 kinase inhibitor [47] showed synergistic cell killing effects against PIM inhibitor-sensitive MOLM-16 and EOL-1 cells (Figure 5A). In OCI-M1 cells, synergy was also observed between

AZD1208 and BMH-21, although a relatively high AZD1208 concentration was required, due to the intrinsic resistance of OCI-M1 cell to PIM kinase inhibition (Figure 5A). To determine whether the combination of AZD1208 and BMH-21 would have a significantly greater therapeutic effect *in vivo*, flank EOL-1 tumors were established in NSG mice. Both AZD1208 and BMH-21 treatment alone significantly reduced the rate of tumor growth compared to vehicle treatment (Figure 5B). Co-treatment with AZD1208 plus BMH-21 was significantly ($p = 0.0366$) more potent than either agent alone in both tumor growth inhibition. These data demonstrate potentiation between AZD1208 and BMH-21 in reducing the rate of EOL-1 tumor growth *in vivo*. In addition, the combination also significantly increased overall survival (Figure 5C).

Discussion

Despite the clinical success of kinase inhibitor therapies, achieving durable responses remains a formidable challenge [4]. While combinatorial treatments with targeted agents represent a proven avenue to attack this problem through polypharmacology, we submit that a major bottleneck in choosing rational co-therapies is our incomplete knowledge of the substrate repertoire of known oncogenic driver kinases and our complete ignorance of physiological substrates for more than 150 less well-studied kinases [11]. In an effort to expand our knowledge of kinase-substrate relationships, we adapted the reverse in-gel kinase assay to permit rapid, proteome-wide discovery of potential physiological kinase substrates. A major source of confounding background phosphorylation in protein extract-based kinase substrate discovery technologies is endogenous kinase activity, and multiple mitigation strategies have been employed [48–55]. Our

electrophoretic approach virtually eliminates background phosphorylation from endogenous kinases given that they can only access co-migrating proteins, whereas the kinase of interest can access all proteins. Additionally, non-enzymatic, quantitative removal of existing phosphorylation and glycosylation by HF treatment ensures the “openness” of phosphoacceptor sites to maximize assay sensitivity [23]. To our knowledge no other kinase-substrate profiling method incorporates a de-glycosylation step, despite the well-documented tension between phosphorylation and glycosylation *in vivo* [56].

Application of the RIKA approach to PIM1 essentially doubled the number of putative substrates. However, as in all *in vitro* proteomic kinase substrate discovery assays that eliminate cellular compartmentalization, establishing the *bona fides* of these putative relationships demands further experimental validation [57]. PIM kinases are known to be both nuclear and cytoplasmic, with potential to access a broad swath of the proteome, and well-studied substrates are found in both compartments [58]. To satisfy a key (albeit *in vitro*) criterion for establishing the validity of putative kinase-substrate relationships, we demonstrated that 19/20 recombinant nuclear and cytoplasmic candidate PIM substrates were robustly phosphorylated by PIM kinases in standard kinase assays [57]. These data also augur favorably for the accuracy of our MS/MS identification workflow for establishing protein identities. Moreover, assignment of substrates into distinct pathways argues strongly for the physiological relevance of a substantial proportion of these putative kinase-substrate relationships. Most importantly, the demonstration that perturbing PIM kinase activity reproducibly alters the output of cellular processes predicted by the pathway analysis to be directly associated

with PIM kinase activity provides functional data in living cells that further substantiates physiological relevance. It is important to note that we cannot, without extensive further time- and resource-intensive investigation, determine precisely what fraction of the substrates reported here may not, under any physiological condition, in any cell population, be directly phosphorylated by PIM kinases *in vivo*. Given that our identification process requires in-gel protein refolding, it is likely that some phospho-acceptor sites on partially refolded proteins could be “falsely” phosphorylated in the assay. Despite this limitation, it is unequivocal that the analysis of our substrate dataset generated rational, actionable, pathway-based leads for combinatorial therapies that synergized to kill AML cells, nominating new treatments for further preclinical development and providing a paradigm to discover co-therapeutics for other kinase inhibitors using this functional validation approach.

The apparent convergence of PIM kinase activity on proteins associated with RNA biology is striking. Of the 461 novel PIM substrates we identified, >250 are classified as RNA-binding proteins. Of these, 65 have been associated with nearly all aspects of mRNA splicing. This highly regulated process initiates during RNA polymerase II transcription and through alternative splicing, ultimately encodes a proteome with a complexity of species that far exceeds the number of annotated protein-coding genes. Several kinase families have long been known to regulate splicing including SR-protein kinases (SRPKs), Cyclin-dependent-like kinases (CLKs), as well as PRP4 kinase, NEK2 kinase, and AKT [59]. Activity of these kinases comprises a complex splicing-regulatory network that is often substantially altered in cancers, with some, for example, SRPK1, having both oncogenic and tumor

suppressive functions (reviewed in [59]). To our knowledge, PIM kinases have not been reported to play a major splicing-regulatory role, however the breadth of putative substrates reported here that are involved in this process, and the extensive changes in splicing observed upon inhibition in AML cell lines strongly implicate PIM family kinases as splicing modulators. Despite the fact PIM kinase activity is not required for viability in mice [60], the strong synergy in cell killing we observed between the SRPK inhibitor SPHINX31 and PIM inhibitors demonstrates that, in at least some cases, AML cells depend on the combined activity of SRPK and PIM kinases for survival. ~~These data provide a clear rationale for combining PIM inhibitors with splicing disruptors in AML.~~ Although based on a limited number of cell lines, these data suggest that the combination of PIM inhibitors and splicing disruptors warrants further investigation as a potential treatment option for some AML patients. Future experiments using patient samples will be critical in establishing the clinical viability of this approach. In addition, given that specific and quantifiable changes in alternative splicing were restricted to PIM inhibitor-responsive cell lines, a panel of splicing changes could potentially serve as a pharmacodynamic biomarker of PIM inhibitor responsiveness.

The PIM kinase substrate repertoire reported here includes 50 proteins implicated in ribosome biogenesis and blocking PIM activity in AML cells resulted in highly reproducible changes in rRNA processing. The diminution of the 26S species is particularly noteworthy. 26S pre-rRNA is generated by endonucleolytic cleavage of the 30S pre-rRNA at a site termed A0 [61]. Recent evidence suggests that UTP23, a putative PIM substrate reported here, is responsible [62]. We speculate that PIM phosphorylation may be required for full UTP23 function in AML cells. Collectively,

alterations in rRNA processing resulting from PIM kinase substrate hypo-phosphorylation can potentially account for the strong synergy in AML cell killing we observed between PIM and RNA Polymerase I inhibitors *in vitro*, and the potentiation of tumor growth inhibition *in vivo*. The synergy observed in AML is also consistent with recent studies demonstrating that PIM inhibition cooperates with Pol I inhibition to block growth of MYC-driven prostate cancers [63].

The approach reported here highlights the merits of illuminating kinases functions by expanding knowledge of their potential physiological substrates to inform new therapeutic approaches and nominate pharmacodynamic biomarkers. Given the strong linkage between aberrant kinase activity and malignant disease, extending this strategy across the kinome can yield mechanistic insights that identify new drug combinations to improve patient outcomes.

Acknowledgements

This work was supported by a 2018 UMBC Technology Catalyst Fund award to C.J.B. The authors thank Flow Cytometry Shared Service of the University of Maryland Marlene and Stewart Greenebaum Comprehensive Cancer Center for assistance with flow cytometric analyses. This publication was supported by funds through the Maryland Department of Health's Cigarette Restitution Fund Program – CH-649-CRF and the National Cancer Institute - Cancer Center Support Grant (CCSG) - P30CA134274.

Author contributions

Conceptualization, T.J., A.C, X.L., and C.J. B.; investigation, T.J., A.C., X.L., A.R., W.H. and A.R.; formal analysis, T. J., A.C., SW.H., X.L., A. V-K., M.R, B.S., X.F. and C.J.B.; resources, T.W. M.L., and M.K.; writing – original draft, T.J., X.L., and C.J. B.; writing – review & editing, all authors; funding acquisition, X.L. and C.J.B.

Declarations

Ethics

The animal studies were performed under a protocol approved by the Institutional Animal Care and Use Committee of the University of Maryland, Baltimore County

Competing interests

The authors declare no competing interests.

Figure titles and legends

Figure 1. Shotgun RIKA nominates PIM-controlled pathways and potential physiological substrates.

(A) RIKA workflow to survey the cellular proteome for protein substrates of PIM1.

(B) Top 10 pathways nominated by DAVID analysis of 778 PIM substrates identified in K562 cell extracts. P-values were calculated for all PIM involved pathways. The top 10, based on P-value and the presence of more than 10 genes in each pathway, were

plotted. Distance of each pathway from center reflects the average enrichment (further = more enriched) and pathway circle area is proportional to the number of pathway proteins. Gene ontology analysis was performed with DAVID database, as described by Huang *et al.* [64]. Kinase substrates identified by mass spectrometry were used for gene over-representation analysis. An enrichment *p*-value of < 0.05 was used in the enriched functional annotation to identify significant biological processes associated with identified kinase substrates.

(C) Top, autoradiogram of standard RIKA analysis of recombinant putative PIM substrates. Left, PIM2-containing gel, right, control gel without PIM2; Bottom, Coomassie Blue-stained RIKA gels from which autoradiograms were obtained. Identical results were obtained with PIM1 containing gels. PIM2 has a lower degree of autophosphorylation compared to PIM1, resulting in higher signal-to-noise in a RIKA.

Figure 2. PIM inhibition alters RNA splicing in AML cell lines.

(A) Quadrant plot of PIM inhibitor-induced splicing index changes for 2,427 events occurring in EOL-1 and MOLM-16 cells. Quadrant 1, up in MOLM-16, down in EOL-1; quadrant 2, up in MOLM-16 & EOL-1; quadrant 3, down in MOLM-16, down in EOL-1; quadrant 4, down in MOLM16, up in EOL-1.

(B) Incidence of alternative splicing events by type in AZD1208-treated MOLM-16 and EOL-1 cells.

(C) TaqMan® qRT-PCR validation of microarray data for MCL-1L and MCL-1S isoforms in AZD1208-treated MOLM-16 and EOL-1 cells. Normalized expression (mean *C_q* from three biological replicates) with SEM is plotted. Data analysis was performed in BioRad

CFX Manager 3.1., and significance values (p -value) of normalized relative expression of MCL-1S to MCL-1L are displayed for one-way ANOVA comparisons with $p < 0.05$.

(D) RT-PCR to detect CHAC1 alternative splicing in PIM-inhibitor-treated MOLM16 or EOL1 cells.

Figure 3. PIM inhibitors synergize with splicing disruptors to kill AML cell lines.

(A) MOLM16 and EOL-1 cells were treated with AZD1208 and Sudemycin D6 or pladienolide B or each drug alone at five doses in the ratios shown.

(B) MLL-rearranged EOL-1 and MV4-11 cells were treated with PIM447 + SPHINX31 or each drug alone at five doses in the ratios shown.

Combination index (CI) values were calculated using CompuSyn. Fa-CI plots were generated based on constant dose ratio drug combination data. $CI < 1$ = synergy; $CI > 1$ = antagonism; $CI = 1$ = additivity. Yellow shaded area indicates synergy and strong effect ($Fa > 0.75$).

Figure 4: PIM inhibition results in pre-rRNA processing defects.

(A) Schematic showing pre-rRNA isoforms and position of internal transcribed spacer (ITS) 1 (salmon vertical bar) and 2 (yellow vertical bar) probes. Mature rRNA sequences within precursors are depicted as blue rectangular boxes, spacers depicted as black lines. Adapted from Tafforeau *et al.*, with permission [45].

(B). Northern blot analysis for AZD1208-treated MOLM-16 and EOL-1 cells using ITS1 (left) and ITS2 (right) probes. Autoradiograms showing ITS1 probe hybridization are presented at two different exposures (top and bottom panels) to permit optimal

visualization of all rRNA intermediates. *, aberrant 18S-E intermediate. 18S rRNA abundance was analyzed by methylene blue staining of Northern membranes.

Figure 5. PIM inhibitors synergize with disruptors of ribosome biogenesis to kill AML cell lines *in vitro* and potentiate growth rate inhibition *in vivo*.

(A) AML cell lines were treated with AZD1208 and BMH-21 (left) or AZD1208 and S6 kinase inhibitor LY2584702 or each drug alone at five doses in the ratios shown. Fa, fraction affected.

(B) Tumor growth rates were calculated for EOL-1 tumors shown in (B). Mean tumor growth rates (mm³/day) were as follows: Control (vehicle treatment) = 0.1212; AZD1208 = 0.0967; BMH-21 = 0.0983; AZD1208 + BMH-21 = 0.0822. Asterisk (*) indicates a statistically significant difference between the average of the mean tumor growth rates of AZD1208- and BMH-21-treated mice versus AZD1208 + BMH-21 (*t*-test, *p* = 0.0366). Statistical analysis of tumor growth rates: We assumed that tumor volume follows an exponential growth model as described [65]:

$$\log_{10} V = a + b \times \text{days} + \epsilon \# (\text{Eq 1})$$

where V is the tumor volume, a and b are parameters of interest, and ϵ is an error term, which has a normal distribution with equal variance for each observation. For four different groups including control group, we estimated a and b from Eq 1, then computed the mean of growth rates. We denote μ_{T_A} , μ_{T_B} , $\mu_{T_{AB}}$ and μ_C to be the mean growth rate for each of three treatment groups (A = AZD1208, B = BMH-21, AB = AZD1208 + BMH-21) and one for control group (C = DMSO), respectively. For instance, $\mu_{T_A} = (1/n_A) \sum_{i=1}^n \hat{b}_i \mathbf{I}_{(i \in A)}$, where n_A is the number of mice in group A, \hat{b}_i is the estimate

of b for i -th mouse, and \mathbf{I} is an indicator function. $n_C = 9$, $n_A = 12$, $n_B = 9$, and $n_{AB} = 9$, which amounts to $n = n_C + n_A + n_B + n_{AB} = 39$ samples in total. We interpret \hat{b}_i as a growth rate of i -th observation, in other words, one expects that it may vary according to the group which i -th mouse belongs to. We then carried out a two-sample t -test to identify whether a significant difference exists among each of treatment groups and control group. We tested

$$H_0: \mu_C = \mu_j$$

$$H_A: \mu_C > \mu_j,$$

where $j=A,B,AB$. We concluded that the growth rate of the control group was significantly higher than the growth rate of any of treatment group on average with 95% confidence level (p -values <0.05).

The mean growth rates were as follows: $\mu_{T_A} = 0.0967$, $\mu_{T_B} = 0.0982$, $\mu_{T_{AB}} = 0.0822$, and $\mu_C = 0.1212$. μ_{T_A} and μ_{T_B} did not appear to be statistically significantly different from each other. We provide the mean of predicted tumor volumes \hat{V} according to time, $\hat{V} = 10^{\hat{a} + \hat{b} \times \text{days}}$ in Figure 5 which shows the similarity in predicted tumor volumes for groups A and B . The t -test confirmed that there is no growth rate difference between A and B : the p -value for testing $H_0: \mu_A = \mu_B$, $H_A: \mu_A \neq \mu_B$ was >0.05 . To determine if the therapeutic effect of AZD1208 + BMH-21 was statistically significantly greater than AZD1208 or BMH-21 alone, we compared the tumor growth rate in groups AB , A , and B . We tested this by conducting a t -test to determine whether the growth rate of AB is statistically significantly lower than those of A and B . Since it was shown that there is no difference between A and B , we performed the following t -test

$$H_0: \mu_{A \cup B} = \mu_{AB}$$

$$H_A: \mu_{A \cup B} > \mu_{AB},$$

where $\mu_{A \cup B}$ is the mean growth rate of both of A and B , i.e., $\mu_{A \cup B} = \{1/(n_A + n_B)\} \sum_{i=1}^n \hat{b}_i \mathbf{I}_{(i \in A \cup B)}$. This test yielded a p -value of <0.05 , hence, we concluded that AZD1208 + BMH-21 reduced the tumor growth rate significantly, compared to the effectiveness of AZD1208 or BMH-21 alone.

(C) Kaplan Meier graph for survival. AZD1208 + BMH-21 extends survival significantly compared to AZD1208 alone ($p = 0.0032$) or BMH-21 alone ($p = 0.0039$).

References

1. Lemmon MA, Schlessinger J. Cell Signaling by Receptor Tyrosine Kinases. *Cell*. 2010;141:1117–34.
2. Bhullar KS, Lagaron NO, McGowan EM, Parmar I, Jha A, Hubbard BP, et al. Kinase-targeted cancer therapies: progress, challenges and future directions. *Mol Cancer*. 2018;17:48.
3. Roskoski R. Properties of FDA-approved small molecule protein kinase inhibitors. *Pharmacol Res*. 2019;144:19–50.

4. Harrison PT, Huang PH. Exploiting vulnerabilities in cancer signalling networks to combat targeted therapy resistance. *Essays Biochem.* 2018;62:583–93.
5. Long GV, Stroyakovskiy D, Gogas H, Levchenko E, Braud F de, Larkin J, et al. Combined BRAF and MEK inhibition versus BRAF inhibition alone in melanoma. *New Engl J Medicine.* 2014;371:1877–88.
6. Duncan JS, Whittle MC, Nakamura K, Abell AN, Midland AA, Zawistowski JS, et al. Dynamic reprogramming of the kinome in response to targeted MEK inhibition in triple-negative breast cancer. *Cell.* 2012;149:307–21.
7. Han K, Jeng EE, Hess GT, Morgens DW, Li A, Bassik MC. Synergistic drug combinations for cancer identified in a CRISPR screen for pairwise genetic interactions. *Nat Biotechnol.* 2017;35:463–74.
8. Griner LAM, Guha R, Shinn P, Young RM, Keller JM, Liu D, et al. High-throughput combinatorial screening identifies drugs that cooperate with ibrutinib to kill activated B-cell-like diffuse large B-cell lymphoma cells. *Proc National Acad Sci.* 2014;111:2349–54.
9. He L, Tang J, Andersson EI, Timonen S, Koschmieder S, Wennerberg K, et al. Patient-Customized Drug Combination Prediction and Testing for T-cell Prolymphocytic Leukemia Patients. *Cancer Res.* 2018;78:2407–18.
10. Venkatesha SH. Methods to Profile Protein Kinase Substrates in Cells. *MOJ Proteomics & Bioinformatics.* 2016;4:1–4.

11. Needham EJ, Parker BL, Burykin T, James DE, Humphrey SJ. Illuminating the dark phosphoproteome. *Sci Signal*. 2019;12:eaau8645.
12. Johnson SA, Hunter T. Kinomics: methods for deciphering the kinome. *Nat Methods*. 2005;2:17–25.
13. Mondello P, Cuzzocrea S, Mian M. Pim kinases in hematological malignancies: where are we now and where are we going? *J Hematol Oncol*. 2014;7:95.
14. Narlik-Grassow M, Blanco-Aparicio C, Carnero A. The PIM family of serine/threonine kinases in cancer. *Med Res Rev*. 2014;34:136–59.
15. Mikkers H, Nawijn M, Allen J, Brouwers C, Verhoeven E, Jonkers J, et al. Mice deficient for all PIM kinases display reduced body size and impaired responses to hematopoietic growth factors. *Mol Cell Biol*. 2004;24:6104–15.
16. Jeyapal GP, Chandrasekar MJN, Krishnasamy R, Selvaraj J, Mohammad M, Nanjan MJ. Potential Pharmacological Inhibitors of Pim Kinase Under Clinical Trials. *Anti-cancer Agent Me*. 2018;18:1100–14.
17. Yang Q, Chen LS, Gandhi V. Mechanism-based combinations with Pim kinase inhibitors in cancer treatments. *Curr Pharm Des*. 2014;20:6670–81.
18. Natarajan K, Bhullar J, Shukla S, Burcu M, Chen Z-S, Ambudkar SV, et al. The Pim kinase inhibitor SGI-1776 decreases cell surface expression of P-glycoprotein (ABCB1) and breast cancer resistance protein (ABCG2) and drug transport by Pim-1-dependent and -independent mechanisms. *Biochem Pharmacol*. 2013;85:514–24.

19. Mumenthaler SM, Ng PYB, Hodge A, Bearss D, Berk G, Kanekal S, et al. Pharmacologic inhibition of Pim kinases alters prostate cancer cell growth and resensitizes chemoresistant cells to taxanes. *Mol Cancer Ther.* 2009;8:2882–93.
20. Xie Y, Xu K, Linn DE, Yang X, Guo Z, Shimelis H, et al. The 44-kDa Pim-1 Kinase Phosphorylates BCRP/ABCG2 and Thereby Promotes Its Multimerization and Drug-resistant Activity in Human Prostate Cancer Cells. *J Biol Chem.* 2008;283:3349–56.
21. Toth RK, Warfel NA. Targeting PIM Kinases to Overcome Therapeutic Resistance in Cancer. *Mol Cancer Ther.* 2021;20:3–10.
22. Li X, Guan B, Srivastava MK, Padmanabhan A, Hampton BS, Bieberich CJ. The reverse in-gel kinase assay to profile physiological kinase substrates. *Nat Methods.* 2007;4:957–62.
23. Li X, Rao V, Jin J, Guan B, Anderes KL, Bieberich CJ. Identification and Validation of Inhibitor-Responsive Kinase Substrates Using a New Paradigm To Measure Kinase-Specific Protein Phosphorylation Index. *J Proteome Res.* 2012;11:3637–49.
24. Swaney DL, McAlister GC, Coon JJ. Decision tree–driven tandem mass spectrometry for shotgun proteomics. *Nat Methods.* 2008;5:959–64.
25. Eng JK, Fischer B, Grossmann J, Maccoss MJ. A fast SEQUEST cross correlation algorithm. *J Proteome Res.* 2008;7:4598–602.

26. Dorfer V, Pichler P, Stranzl T, Stadlmann J, Taus T, Winkler S, et al. MS Amanda, a Universal Identification Algorithm Optimized for High Accuracy Tandem Mass Spectra. *J Proteome Res.* 2014;13:3679–84.
27. Käll L, Canterbury JD, Weston J, Noble WS, MacCoss MJ. Semi-supervised learning for peptide identification from shotgun proteomics datasets. *Nat Methods.* 2007;4:923–5.
28. Taus T, Köcher T, Pichler P, Paschke C, Schmidt A, Henrich C, et al. Universal and confident phosphorylation site localization using phosphoRS. *J Proteome Res.* 2011;10:5354–62.
29. Li X, Cox JT, Huang W, Kane M, Tang K, Bieberich CJ. Quantifying Kinase-Specific Phosphorylation Stoichiometry Using Stable Isotope Labeling In a Reverse In-Gel Kinase Assay. *Anal Chem.* 2016;88:11468–75.
30. Orsburn BC. Proteome Discoverer-A Community Enhanced Data Processing Suite for Protein Informatics. *Proteomes.* 2021;9:15.
31. Hornbeck PV, Zhang B, Murray B, Kornhauser JM, Latham V, Skrzypek E. PhosphoSitePlus, 2014: mutations, PTMs and recalibrations. *Nucleic Acids Res.* 2014;43:D512-20.
32. Sugiyama N, Imamura H, Ishihama Y. Large-scale Discovery of Substrates of the Human Kinome. *Sci Rep-uk.* 2019;9:10503.

33. Huang DW, Sherman BT, Tan Q, Collins JR, Alvord WG, Roayaei J, et al. The DAVID Gene Functional Classification Tool: a novel biological module-centric algorithm to functionally analyze large gene lists. *Genome Biol.* 2007;8:R183.
34. Keeton EK, McEachern K, Dillman KS, Palakurthi S, Cao Y, Grondine MR, et al. AZD1208, a potent and selective pan-Pim kinase inhibitor, demonstrates efficacy in preclinical models of acute myeloid leukemia. *Blood.* 2013;123:905–13.
35. Saez B, Walter MJ, Graubert TA. Splicing factor gene mutations in hematologic malignancies. *Blood.* 2017;129:1260–9.
36. Lee SC, Dvinge H, Kim E, Cho H, Micol JB, Chung YR, et al. Modulation of splicing catalysis for therapeutic targeting of leukemia with mutations in genes encoding spliceosomal proteins. *Nat Med.* 2016;22:672–8.
37. Kotake Y, Sagane K, Owa T, Mimori-Kiyosue Y, Shimizu H, Uesugi M, et al. Splicing factor SF3b as a target of the antitumor natural product pladienolide. *Nat Chem Biol.* 2007;3:570–5.
38. Lagisetti C, Palacios G, Goronga T, Freeman B, Caufield W, Webb TR. Optimization of antitumor modulators of pre-mRNA splicing. *J Med Chem.* 2013;56:10033–44.
39. Chou T-C, Talalay P. Quantitative analysis of dose-effect relationships: the combined effects of multiple drugs or enzyme inhibitors. *Adv Enzyme Regul.* 1984;22:27–55.

40. Zhou Z, Fu X-D. Regulation of splicing by SR proteins and SR protein-specific kinases. *Chromosoma*. 2013;122:191–207.
41. Aubol BE, Wu G, Keshwani MM, Movassat M, Fattet L, Hertel KJ, et al. Release of SR Proteins from CLK1 by SRPK1: A Symbiotic Kinase System for Phosphorylation Control of Pre-mRNA Splicing. *Mol Cell*. 2016;63:218–28.
42. Tzelepis K, Koike-Yusa H, De Braekeleer E, Li Y, Metzakopian E, Dovey OM, et al. A CRISPR Dropout Screen Identifies Genetic Vulnerabilities and Therapeutic Targets in Acute Myeloid Leukemia. *Cell Reports*. 2016;17:1193–205.
43. Tzelepis K, Braekeleer ED, Aspris D, Barbieri I, Vijayabaskar MS, Liu WH, et al. SRPK1 maintains acute myeloid leukemia through effects on isoform usage of epigenetic regulators including BRD4. *Nat Commun*. 2018;9:5378.
44. Warfel NA, Kraft AS. PIM kinase (and Akt) biology and signaling in tumors. *Pharmacol Therapeut*. 2015;151:41–9.
45. Tafforeau L, Zorbas C, Langhendries J-L, Mullineux S-T, Stamatopoulou V, Mullier R, et al. The Complexity of Human Ribosome Biogenesis Revealed by Systematic Nucleolar Screening of Pre-rRNA Processing Factors. *Mol Cell*. 2013;51:539–51.
46. Peltonen K, Colis L, Liu H, Trivedi R, Moubarek MS, Moore HM, et al. A targeting modality for destruction of RNA polymerase I that possesses anticancer activity. *Cancer cell*. 2014;25:77–90.

47. Tolcher A, Goldman J, Patnaik A, Papadopoulos KP, Westwood P, Kelly CS, et al. A phase I trial of LY2584702 tosylate, a p70 S6 kinase inhibitor, in patients with advanced solid tumours. *Eur J Cancer*. 2014;50:867–75.
48. Ptacek J, Devgan G, Michaud G, Zhu H, Zhu X, Fasolo J, et al. Global analysis of protein phosphorylation in yeast. *Nature*. 2005;438:679–84.
49. Cohen P, Knebel A. KESTREL: a powerful method for identifying the physiological substrates of protein kinases. *Biochem J*. 2005;393:1–6.
50. Amano M, Hamaguchi T, Shohag MH, Kozawa K, Kato K, Zhang X, et al. Kinase-interacting substrate screening is a novel method to identify kinase substrates. *J Cell Biology*. 2015;209:895–912.
51. Embogama DM, Pflum MKH. K-BILDS: A Kinase Substrate Discovery Tool. *Chembiochem*. 2016;18:136–41.
52. Müller AC, Giambruno R, Weißer J, Májek P, Hofer A, Bigenzahn JW, et al. Identifying Kinase Substrates via a Heavy ATP Kinase Assay and Quantitative Mass Spectrometry. *Sci Rep-uk*. 2016;6:28107.
53. Shah K, Liu Y, Deirmengian C, Shokat KM. Engineering unnatural nucleotide specificity for Rous sarcoma virus tyrosine kinase to uniquely label its direct substrates. *Proc National Acad Sci*. 1997;94:3565–70.

54. Nishioka T, Nakayama M, Amano M, Kaibuchi K. Proteomic Screening for Rho-kinase Substrates by Combining Kinase and Phosphatase Inhibitors with 14-3-3 ζ Affinity Chromatography. *Cell Struct Funct.* 2012;37:39–48.
55. Xue L, Wang W-H, Iliuk A, Hu L, Galan JA, Yu S, et al. Sensitive kinase assay linked with phosphoproteomics for identifying direct kinase substrates. *P Natl Acad Sci Usa.* 2012;109:5615–20.
56. Laarse SAM, Leney AC, Heck AJR. Crosstalk between phosphorylation and O-GlcNAcylation: friend or foe. *Febs J.* 2018;285:3152–67.
57. Krebs EG, Beavo JA. Phosphorylation-dephosphorylation of enzymes. *Annual review of biochemistry.* 1979;48:923–59.
58. Santio NM, Koskinen PJ. PIM kinases: From survival factors to regulators of cell motility. *Int J Biochem Cell Biology.* 2017;93:74–85.
59. Czubaty A, Piekuelko-Witkowska A. Protein kinases that phosphorylate splicing factors: Roles in cancer development, progression and possible therapeutic options. *Int J Biochem Cell Biology.* 2017;91:102–15.
60. An N, Kraft AS, Kang Y. Abnormal hematopoietic phenotypes in Pim kinase triple knockout mice. *J Hematol Oncol.* 2013;6:12.
61. Mullineux S-T, Lafontaine DLJ. Mapping the cleavage sites on mammalian pre-rRNAs: Where do we stand? *Biochimie.* 2012;94:1521–32.

62. Wells GR, Weichmann F, Sloan KE, Colvin D, Watkins NJ, Schneider C. The ribosome biogenesis factor yUtp23/hUTP23 coordinates key interactions in the yeast and human pre-40S particle and hUTP23 contains an essential PIN domain. *Nucleic Acids Res.* 2017;gkw1344.
63. Rebello RJ, Kushnadi E, Cameron DP, Pearson HB, Lesmana A, Devlin JR, et al. The Dual Inhibition of RNA Pol I Transcription and PIM Kinase as a New Therapeutic Approach to Treat Advanced Prostate Cancer. *Clin Cancer Res.* 2016;22:5539–52.
64. Huang DW, Sherman BT, Lempicki RA. Systematic and integrative analysis of large gene lists using DAVID bioinformatics resources. *Nat Protoc.* 2009;4:44–57.
65. Hather G, Liu R, Bandi S, Mettetal J, Manfredi M, Shyu W-C, et al. Growth rate analysis and efficient experimental design for tumor xenograft studies. *Cancer Informatics.* 2014;13:65–72.

Figure 1
FIGURE 1

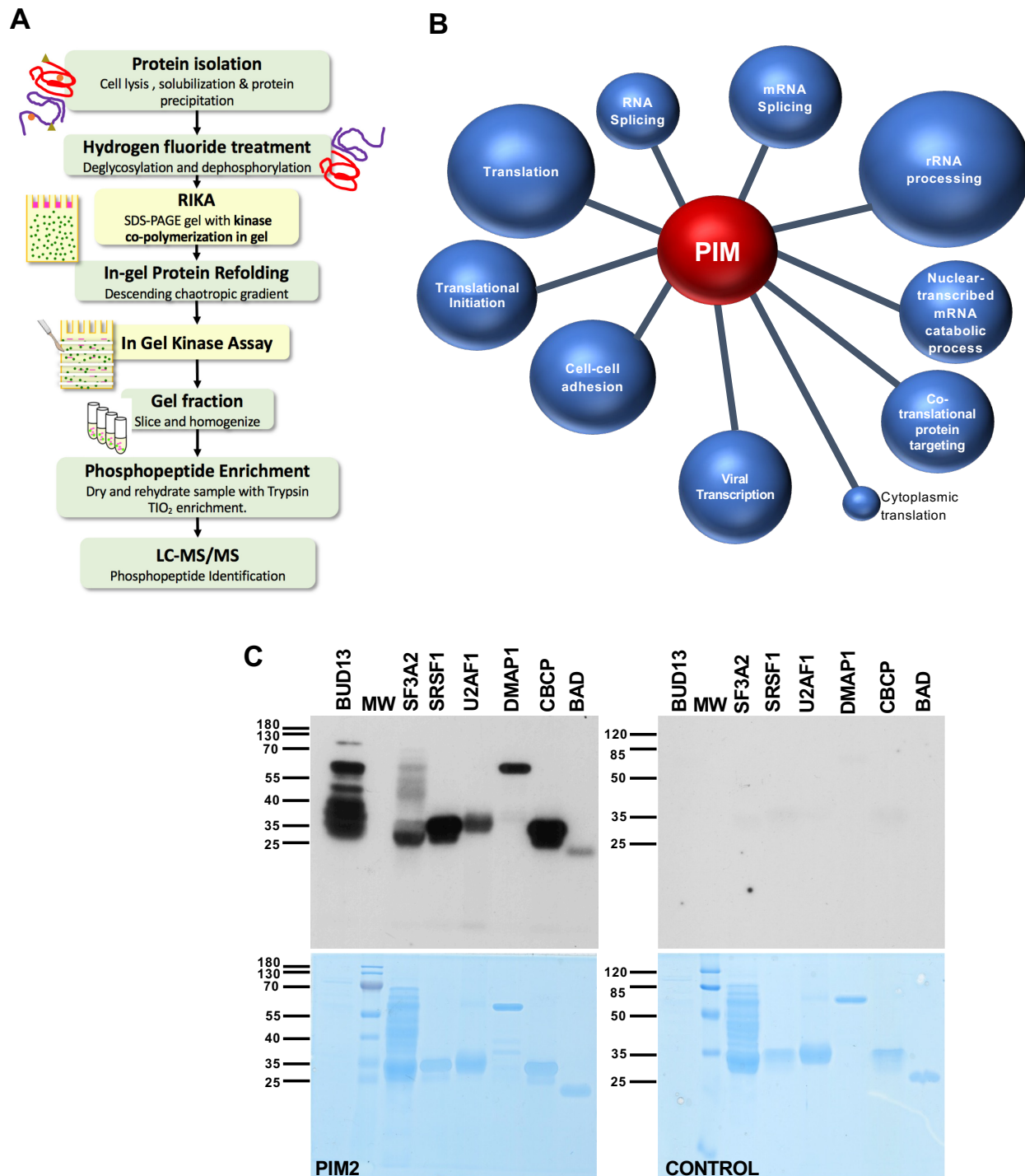


Figure 2
FIGURE 2

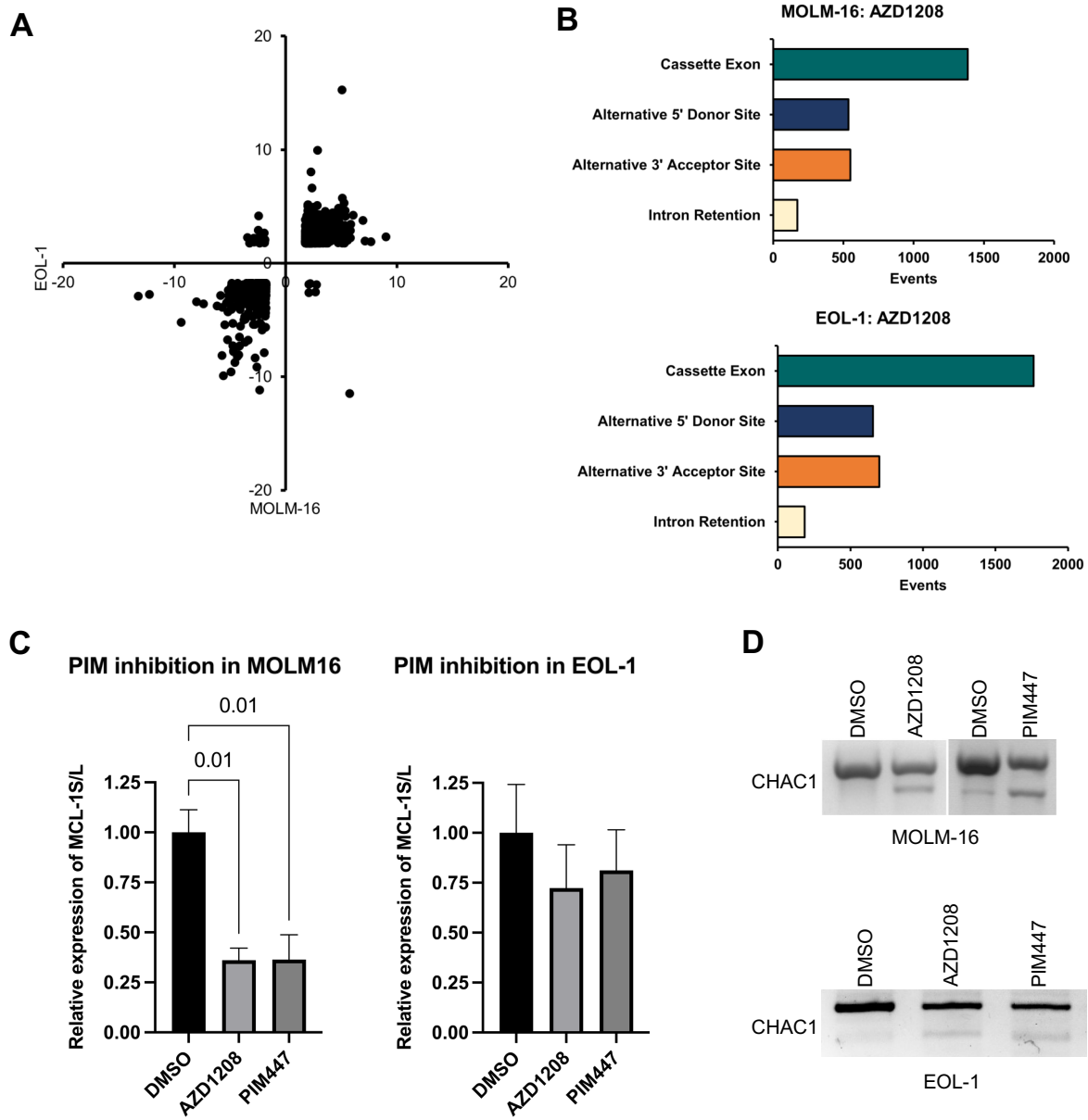


Figure 3
FIGURE 3

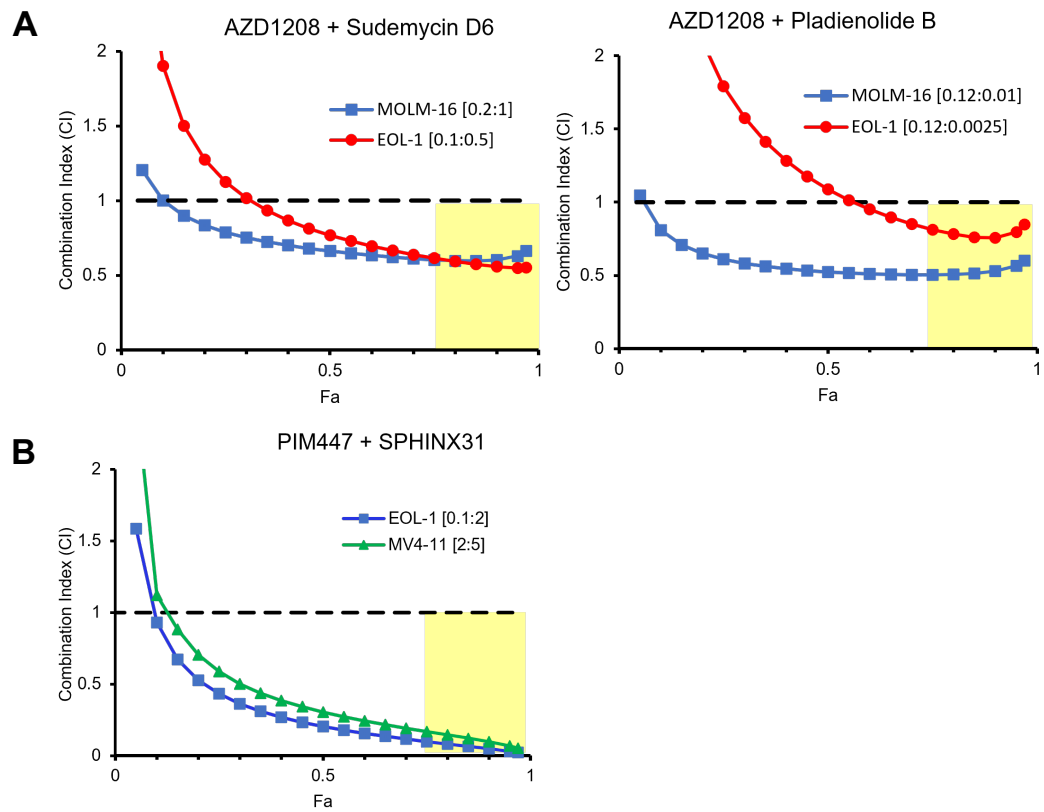


Figure 4
FIGURE 4

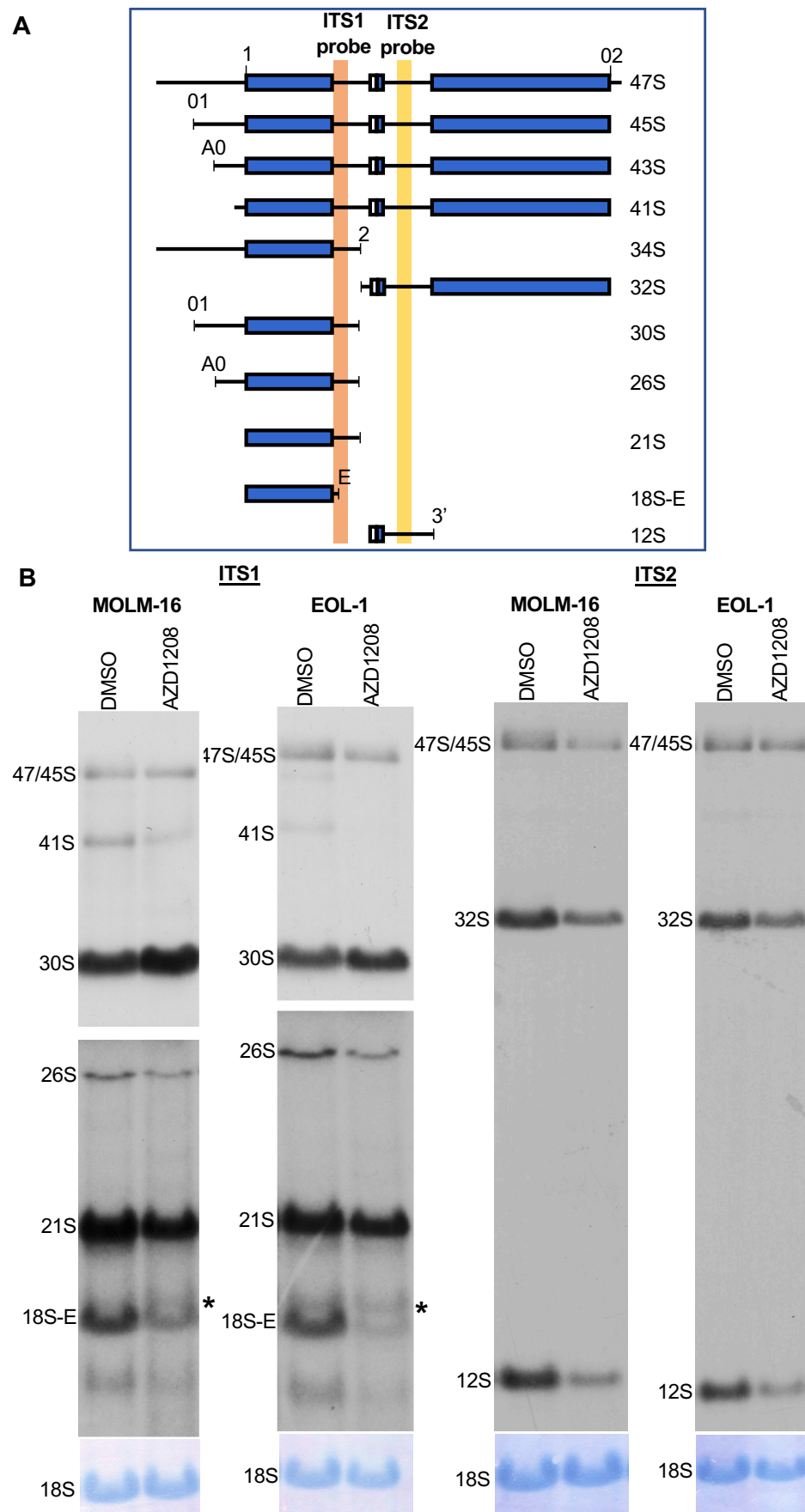


Figure 5
FIGURE 5

